

Probing the spin-induced quadrupole moment of massive black holes with the inspiral of binary black holes

Ying-Lin Kong (孔英燦)[✉] and Jian-dong Zhang (张建东)^{✉*}

MOE Key Laboratory of TianQin Mission, TianQin Research Center for Gravitational Physics and School of Physics and Astronomy, Frontiers Science Center for TianQin, Gravitational Wave Research Center of CNSA, Sun Yat-sen University (Zhuhai Campus), Zhuhai 519082, China



(Received 23 January 2024; accepted 25 June 2024; published 23 July 2024)

One of the most important sources for space-borne gravitational wave detectors such as TianQin and the Laser Interferometer Space Antenna is the merger of massive black hole binaries. By analyzing the inspiral signals, we can probe the characteristics of massive black holes, including the spin-induced multipole moments. By verifying the relation among mass, spin, and quadrupole moment, the no-hair theorem can be tested. In this work, we analyzed the capability of probing the spin-induced quadrupole moment with the inspiral signal of massive black hole binaries using space-borne gravitational wave detectors. Using the Fisher information matrix, we find that the deviation of the quadrupole moment can be constrained to the level of 10^{-1} , and events with higher mass ratios will provide a better constraint. We also find that the late inspiral part will dominate the result of parameter estimation. The results of Bayesian analysis indicate that the capability will be significantly enhanced by considering higher modes. We also calculate the Bayes factor, and the results indicate that the model of a black hole and a boson star can be distinguished without a doubt.

DOI: [10.1103/PhysRevD.110.024059](https://doi.org/10.1103/PhysRevD.110.024059)

I. INTRODUCTION

After the first detection of the gravitational wave (GW) from GW150914 [1], the LIGO-Virgo-KAGRA Collaboration has already reported 90 events involving the merger of stellar mass compact binaries [2–5], which include binary black hole (BBH), binary neutron star, and neutron star–black hole [5,6]. Besides black holes (BHs) and neutron stars (NSs), some models of exotic objects [7] such as quark stars [8], boson stars (BSs) [9], gravastars [10], and BHs in modified theories of gravity are also proposed as alternatives [11]. The GWs generated by the binaries constituted of these exotic compact objects (ECOs) will differ from those produced by BBHs. Therefore, we can use GWs to test the nature of compact objects.

According to the black hole no-hair theorem [12], the classical black holes in general relativity are fully characterized by their masses, spins, and charges. However, due to various neutralization mechanisms [13], it is widely believed that astrophysical BHs will have negligible electric charge. So these BHs can be characterized by the Kerr metric, which includes only the mass M and the spin a as the parameters. By measuring multiple parameters of a BH and testing if they could provide a consistent prediction of M and a according to general relativity, we can test the no-hair theorem and probe the nature of compact objects.

Various parametrization methods have been proposed for such tests, including tidal deformability [14–17], the horizon absorption effect [18], the quasinormal mode spectrum of ringdown [19–27], and multipole moments [28,29]. With these parametrizations, the BH will perform differently compared to the mimickers.

For a localized object, its gravitational field can be expanded in terms of the multipole moments [30–33]. For stationary asymptotically flat solutions of the Einstein equation, such as the Kerr black hole, the multipole moments can be expressed by the mass M and spin a as

$$\mathcal{M}_l + i\mathcal{S}_l = M(ia)^l. \quad (1)$$

There are two sets of multipole moments: the mass moments \mathcal{M}_l for even l 's and the current moments \mathcal{S}_l for odd l 's. The mass multipole moments for odd orders and the current multipole moments for even orders will vanish due to the equatorial symmetry of the Kerr solution. The leading-order mass moment $\mathcal{M}_0 = M$ and current moment $\mathcal{S}_1 = Ma$ are the mass and spin angular momentum of the Kerr BH, respectively. If we can measure the multipole moments with $l \geq 2$ besides the mass and spin, then we can test if these expressions are broken and, thus, test the no-hair theorem.

In most cases, only the $l = 2$ term, known as the spin-induced quadrupole moment (SIQM), is considered in the relevant test. For a general compact object, the SIQM can

*Contact author: zhangjd9@mail.sysu.edu.cn

be represented as $Q = -\kappa\chi^2 M^3$, where $\chi = a/M$ is the dimensionless spin parameter and κ is a coefficient that depends on the internal structure of the object related to its equation of state [34]. For BHs, we will have $\kappa = 1$ according to (1). For NSs, it is believed that κ can vary between 2 and 14 [35,36] due to the multipole deformation that occurs during the rotation process [37], up to quadratic in spin. For BSs, the range of κ is about 10–150 [38,39]. For some other BH mimickers such as gravastars, the value can also be negative [40,41]. By measuring κ , we can distinguish between the BHs and its mimickers [42,43].

Using the low-mass events in GWTC-2 [44], the data support the model of BBH rather than ECO, and κ is constrained to the order of $\mathcal{O}(10^2)$. Recent work has also analyzed the impact of spin precession and higher modes on the measurement of SIQM [45] and the constraint on octupole moments [46] with ground-based detectors. Some selected GWTC events are also used in the data analysis. The combined Bayesian factor among the GWTC events is calculated: $\log\text{BF}_{\delta\kappa, \neq 0}^{\text{Kerr}} = 0.9$ [47] in GWTC-3 and 1.1 in GWTC-2 [48]. The capability is also analyzed for the Laser Interferometer Space Antenna (LISA) and Deci-hertz Interferometer Gravitational wave Observatory [49] with the detection of massive black hole binary (MBHB), and κ is expected to be constrained to the order of $\mathcal{O}(0.1)$. Based on some astrophysical models for the population of MBHB, it is also argued that 3% of the events can reach these levels. Moreover, with the detection of extreme mass-ratio inspirals (EMRIs), TianQin [50–52] and LISA [53–56] can constrain the SIQM to 10^{-5} .

TianQin is a space-borne GW detector [57,58] to be launched in 2035. It comprises three drag-free satellites orbiting Earth at a radius of 10^5 km and aims to detect GWs on the millihertz band. The major objectives [59] include the merger of MBHBs [60,61], the inspiral of stellar-mass BBHs [62,63], the galactic compact binaries [64], the EMRIs [50,65], and the stochastic GW background [66,67]. With the observation of these signals, we can also study the evolution of the Universe [68–70] and the nature of BHs and gravity [23,51,71–75].

In this work, we conduct a more comprehensive study on the effectiveness of TianQin in testing the no-hair theorem by probing the SIQM with the inspiral signal of MBHBs. According to the result of [60], TianQin is expected to detect about 60 events every year for the most optimistic model. We consider the higher (l, m) mode corrections due to the deviation of the SIQM and utilize time delay interferometry (TDI) response to generate the signal. With the Fisher information matrix (FIM) analysis, we find that the late inspiral will dominate the accuracy of the constraint. This indicates that we do not need to consider a full inspiral signal in this analysis. The results also indicate that events with asymmetric mass will have better capability, and higher modes will be important for events with large mass ratios. So, we also consider these higher modes

in our waveform and the corresponding modifications. Then we use BILBY to conduct the Bayesian analysis, and the accuracy of the parameter estimation is consistent with the FIM result. For the injection signal with a nonzero $\delta\kappa$, if we do not consider this deviation in the matched waveform, the result will exhibit a significant bias in the estimation of other source parameters. By calculating the Bayes factor, we find that the signal from BHs and ECOs can be distinguished without a doubt.

The paper is organized as follows. In Sec. II, we will provide a brief review of the basic methods for waveforms, responses, and statistics in each subsections, respectively. Then, we present our results for TianQin with FIM and Bayesian analysis in Sec. III. Finally, we provide a brief summary of conclusion in Sec. IV. Throughout this work, the geometrized unit system ($G = c = 1$) is used.

II. METHOD

A. Waveform

In this work, we utilize the IMRPhenomXHM [76] waveform, which is a frequency domain model for the inspiral-merger-ringdown of quasicircular nonprecessing BBH with higher modes. In general, the waveform can be expressed as

$$h_{\text{BBH}}(f) = \sum_{lm} A_{lm}(f) e^{i\Psi_{lm}^{\text{BBH}}(f)}. \quad (2)$$

$A_{lm}(f)$ and $\Psi_{lm}^{\text{BBH}}(f)$ are the amplitude and phase for the lm mode, respectively. The index “BBH” indicates that the corresponding formula is derived for BBHs, and it will be different for binaries constituted of ECOs. The SIQM of the progenitors will influence the phase evolution of inspiral, while the remnant SIQM will affect the quasinormal mode spectrum of ringdown. In this work, we will focus on the inspiral phase, and, therefore, a cutoff at the innermost stable circular orbit (ISCO) will be adopted in the subsequent calculations. Since the spin precession is not considered in the waveform we used, we will assume the aligned or antialigned spin for the binaries.

For binaries constituted of ECOs, the waveform for inspiral can be modified:

$$h_{\text{ECO}}(f) = \sum_{lm} A_{lm}(f) e^{i(\Psi_{lm}^{\text{BBH}}(f) + \Psi_{lm}^{\text{SIQM}}(f))}. \quad (3)$$

This implies that we disregard the modification of the amplitude [77], because the phase will have greater impact on the accuracy of parameter estimation (PE) for intrinsic parameters. If we neglect the tidal effect and consider only the leading-order correction of SIQM, the phase correction for the leading 22 mode can be expressed as [34,44,77,78]

$$\Psi_{22}^{\text{SIQM}}(f) = \frac{75 \delta\kappa_1 M_1^2 \chi_1^2 + \delta\kappa_2 M_2^2 \chi_2^2}{64 M_1 M_2} (\pi M_{\text{tot}} f)^{-1/3}. \quad (4)$$

$M_{\text{tot}} = M_1 + M_2$ is the total mass of the binary system, and $\delta\kappa_i = \kappa_i - 1$ characterizes the deviation of the SIQM relative to the BH. It should be noted that the mass we used is the redshifted mass all through this paper. The power index of $-1/3$ means that this leading-order correction emerges at the 2PN order. We set $\delta\kappa_1 = \delta\kappa_2 = \delta\kappa$ and, thus, ignore the antisymmetric contribution. Obviously, the BBH cases correspond to $\delta\kappa = 0$, and we have neglected the BH-ECO system or binary ECOs with different κ .

For the correction of the phase of the higher modes, we utilize the relation provided in the parametrized post-Einsteinian framework [79]. Since the leading-order correction emerges at 2PN order, the higher modes correction can be written as

$$\psi_{lm}^{\text{SIQM}} = \left(\frac{2}{m}\right)^{-4/3} \psi_{22}^{\text{SIQM}}. \quad (5)$$

In our analysis, the modes we considered include the dominant mode (2, 2) and subdominant modes (2, 1) and (3, 3).

B. The response and noise of TianQin

For space-borne GW detectors, TDI [80,81] must be used to suppress the laser phase noise. In this work, we utilized the 1.0-type channel for A , E , and T for data analysis. The signal is obtained by multiplying the waveform with the transfer function:

$$h_{\bar{A}, \bar{E}, \bar{T}} = \sum_{lm} \mathcal{T}_{\bar{A}, \bar{E}, \bar{T}}^{lm} \tilde{h}_{lm}(f). \quad (6)$$

For details on the formalism of the transfer function for TianQin, please refer to [82]. The orbit motion of TianQin is considered as the ideal case described in [57]. Thus, the modulation caused by the rotation of the constellation around Earth, and the Doppler effect caused by the motion of the constellation around the Sun, will be included in the calculation of the response. In this work, we consider only the A channel in our calculations.

The power spectral density for the noise of TianQin corresponding to the TDI channel can be written as

$$S_{A,E} = 8 \sin^2 \frac{f}{f_*} \left[\left(2 + \cos \frac{f}{f_*} \right) (2\pi f)^2 S_x + 4 \left(1 + \cos \frac{f}{f_*} + \cos^2 \frac{f}{f_*} \right) \left(1 + \frac{0.1 \text{ mHz}}{f} \right) \frac{S_a}{(2\pi f)^2} \right], \quad (7)$$

where $f_* = \frac{1}{2\pi L}$ is the characteristic frequency of TianQin and $L = \sqrt{3} \times 10^8$ m is the arm length. The acceleration noise S_a and the position noise S_x are [57], respectively,

$$S_a = 10^{-30} \text{ m}^2 \cdot \text{s}^{-4} \cdot \text{Hz}^{-1}, \\ S_x = 10^{-24} \text{ m}^2 \cdot \text{Hz}^{-1}. \quad (8)$$

C. Parameter estimation

In this study, FIM is used to estimate TianQin's capability to measure the parameters. By the definition of an inner product

$$(g|h) \equiv 2 \int_{f_{\text{low}}}^{f_{\text{high}}} \frac{g(f)^* h(f) + h(f)^* g(f)}{S_n(f)} df, \quad (9)$$

the FIM is defined as [83]

$$\Gamma_{ij} \equiv \left(\frac{\partial h}{\partial \theta_i} \middle| \frac{\partial h}{\partial \theta_j} \right), \quad (10)$$

h is the response signal of the injected waveform, and θ_i is the i th parameter of the source. In our analysis, the parameters are chosen as follows:

$$\theta = \{\mathcal{M}, \eta, D_L, t_c, \phi_c, \psi, \iota, \chi_1, \chi_2, \delta\kappa_s\}. \quad (11)$$

$\eta = \frac{M_1 M_2}{(M_1 + M_2)^2}$ is the symmetric mass ratio, $\mathcal{M} = M_{\text{tot}} \eta^{3/5}$ is the chirp mass, and D_L is the luminosity distance. t_c and ϕ_c represent the time and phase at coalescence, respectively. ψ and ι represent the polarization and inclination angles of the source, respectively. χ_1 and χ_2 represent the dimensionless spin parameters for each BHs. For a signal with a large signal-to-noise ratio (SNR), the uncertainty in parameter estimation is given by

$$\Delta\theta_i = \sqrt{\Gamma_{ii}^{-1}}.$$

In the calculation of the inner product, the lower- and higher-frequency bounds are chosen, respectively, as

$$f_{\text{high}} = \min(f_{\text{max}}, f_{\text{isco}}), \\ f_{\text{low}} = \max(f_{\text{min}}, f_{\text{init}}). \quad (12)$$

Because of the sensitivity band of TianQin, we set $f_{\text{max}} = 1$ Hz and $f_{\text{min}} = 10^{-4}$ Hz, and signals outside of this band will be ignored. The initial frequency of the source f_{init} depends on the time T we begin to observe before the merger of the BBH:

$$f_{\text{init}} = \left(\frac{5}{256} \right)^{3/8} \frac{\mathcal{M}^{-5/8}}{\pi} T^{-3/8}. \quad (13)$$

f_{isco} is the frequency for the ISCO, which marks the end of the inspiral. In our calculation, we use the Kerr frequency instead of Schwarzschild, because spin plays a crucial role in our calculation, and it significantly affects the radius of ISCO. The detailed formalism can be found in the Appendix.

For a more realistic analysis, we also use Bayesian inference [84] to perform PE for simulated data. In the Bayesian framework, the posterior distribution $p(\theta|D)$ for a specific set of parameters θ with the given data D is

$$p(\theta|D) = \frac{p(D|\theta)p(\theta)}{p(D)}. \quad (14)$$

In the equation above, $p(\theta)$ represents the prior, $p(D|\theta)=\mathcal{L}$ represents the likelihood, and $p(D) = \mathcal{Z}$ is the evidence necessary to ensure the normalization condition of the posterior

$$\int p(\theta|d)d\theta = 1. \quad (15)$$

For GW detection, we typically assume that the noise is stationary and Gaussian. In this case, the likelihood can be expressed as

$$\ln \mathcal{L} \propto -\frac{1}{2}(D - h(\theta)|D - h(\theta)). \quad (16)$$

$h(\theta)$ is the waveform template for a given set of parameters θ . The proportionality coefficient is not relevant to θ . The evidence is then defined as

$$\mathcal{Z} = \int \mathcal{L}(D|\theta)p(\theta)d\theta. \quad (17)$$

Beyond the calculation of the posterior, we can also investigate model selection, which involves determining which model is favored by the observed data. This can be achieved by calculating the Bayes factor between two models \mathcal{M}_1 and \mathcal{M}_2 :

$$\text{BF}_2^1 = \frac{\mathcal{Z}_1}{\mathcal{Z}_2}, \quad (18)$$

and \mathcal{Z}_i is the evidence of the model \mathcal{M}_i . The lg Bayes factor is most commonly used, and it is defined as

$$\lg \text{BF}_2^1 = \lg \mathcal{Z}_1 - \lg \mathcal{Z}_2. \quad (19)$$

In the calculation of the posterior distribution, we use BILBY [85] to implement parameter estimation, which is primarily designed for inferring compact binary coalescence events from interferometric data. For sampling across the parameter space, we utilized DYNESTY [86] based on the nested sampling algorithm [87]. However, since BILBY is designed for ground-based detectors, we modified the components related to the response and noise of the detector, as we introduce in Sec. II B.

III. RESULT

The default parameters of the MBHBs we used for both Fisher and Bayesian analysis are shown in Table I. We also list the prior we use in the Bayesian analyses for each parameter in this table. Beside the parameters listed in (11), β and λ represent the latitude and longitude, respectively, for the sources in ecliptic coordinates. Since we consider only the 1-day data in our analysis, the detector's response will not change significantly. Thus, the position of the source that will influence the response is poorly constrained. So, we estimate all the parameters in Table I except β and λ .

A. Fisher analysis on the capability of TianQin

In the sensitive frequency band of TianQin, the inspiral of the MBHBs may last for years before merging. However, it has been found that the late inspiral part will capture most of the SNR [61]. According to the results shown in Table II, we can observe that the signal from the last day contributes 99.9% of the SNR for the entire year. The PE accuracy for 1 month is almost equivalent to the accuracy for 1 year, whereas the accuracy for 1 day is approximately 1.8 times lower than the accuracy for 1 year. So, in the Bayesian analysis which will be discussed in the following subsection, we will consider only the analysis of the data from the final day before the merger to reduce the cost of computation. More over, according to the Fisher analysis with or without β and λ , the accuracies for the constraint on

TABLE I. The default values and the prior of the parameters we choose for the MBHBs.

Parameter	Value	Prior
$\mathcal{M}(M_\odot)$	1.24×10^6	Logarithm uniform $[10^2, 10^8]$
η	$\frac{2}{9}$	Uniform $[\frac{1}{12}, \frac{1}{4}]$
D_L (Mpc)	1000	Quadratic uniform $[10^2, 10^4]$
t_c (s)	3600	Uniform $[-10000, 10000]$
ϕ_c (rad)	$\frac{\pi}{4}$	Uniform $[-\pi, \pi]$
ψ (rad)	$\frac{\pi}{4}$	Uniform $[-\pi, \pi]$
ι (rad)	$\frac{\pi}{4}$	Cosine uniform $[0, \pi]$
χ_1	0.2	Uniform $[-1, 1]$
χ_2	0.1	Uniform $[-1, 1]$
β (rad)	$\frac{\pi}{4}$...
λ (rad)	$\frac{\pi}{4}$...
$\delta\kappa$	0	Uniform $[-20, 20]$

TABLE II. The SNR and PE accuracy for the default source with varying duration.

Duration time	SNR	$\delta\kappa$
1 year	6641.35	0.174
1 month	6641.35	0.174
1 week	6641.16	0.213
1 day	6639.58	0.328

$\delta\kappa$ are almost the same, and the correlation between $\delta\kappa$ and the sky position is very weak. However, the PE for the position of the source is determined by the modulation of the response function which caused by the movement of the detector. If we consider only the data from the last day, the detector will not move significantly, and, thus, the estimate of the position will be very worse.

This can be easily solved by considering a longer data. Since we focus only on the estimation of $\delta\kappa$, and it will not have a correlation with the latitude and longitude of the source, we will ignore these two parameters in the following analysis.

According to the results above, we can see that TianQin can constrain the SIQM to the level of $\mathcal{O}(0.1)$. Then, we calculate the capacity for the sources with different total mass and mass ratio. The result is shown in Fig. 1 as a contour plot. For a fair comparison, the SNR is normalized to 5000 by adjusting the luminosity distance D_L . The mass ratio q varies between 1 and 21, and the total mass varies between $10^4 M_\odot$ and $10^7 M_\odot$.

According to the contour plot, we can see that TianQin has better sensitivity for sources around $10^{5.5} M_\odot$. This region corresponds to the most sensitive band of TianQin. Comparing this with the result of LISA obtained in [49], we can see that LISA has better sensitivity for sources around $2 \times 10^6 M_\odot$, since it is more sensitive for the lower frequencies than TianQin. Similar phenomenons have also been found for other studies of the detection of MBHBs, and more detailed comparison between LISA and TianQin can be found in [88]. It also shows that events with a higher mass ratio will provide better constraints. This is consistent with the result of EMRI [51], where the mass ratio become 10^6 and the constraint of the SIQM reaches the level of 10^{-4} . For events with asymmetric masses, the higher modes

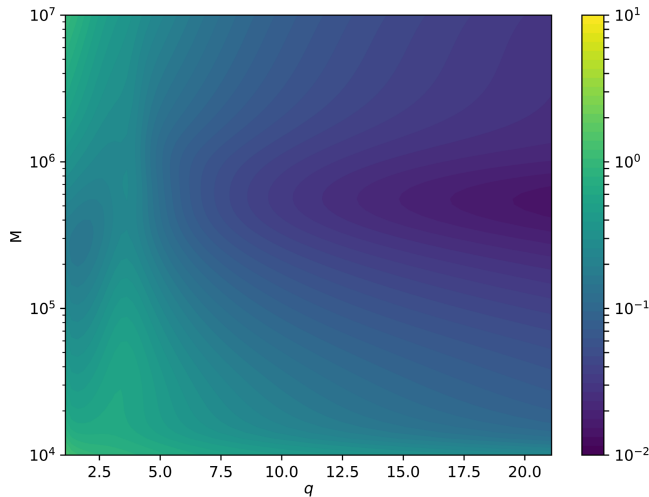


FIG. 1. The contour plot shows the PE accuracy of $\delta\kappa$ for sources with different total mass and mass ratio values over a signal duration of 1 day. The SNR for each point is normalized to 5000 by changing D_L .

will become important. According to previous studies, introducing modifications on the higher modes can also enhance the capability [89]. This will be discussed with Bayesian analysis in the next subsection.

B. Bayesian analysis

For the Bayesian analysis, we consider two types of injected data: The first one is the BBH signal with $\delta\kappa = 0$, and the second one is the binary ECO signal with $\delta\kappa = 10$. It should be noted that the mock data in our analysis are an idealized case. In the real data for space-borne GW detectors, there may exist multiple different kinds of signals at the same time. Thus, a global fit method [90,91] must be

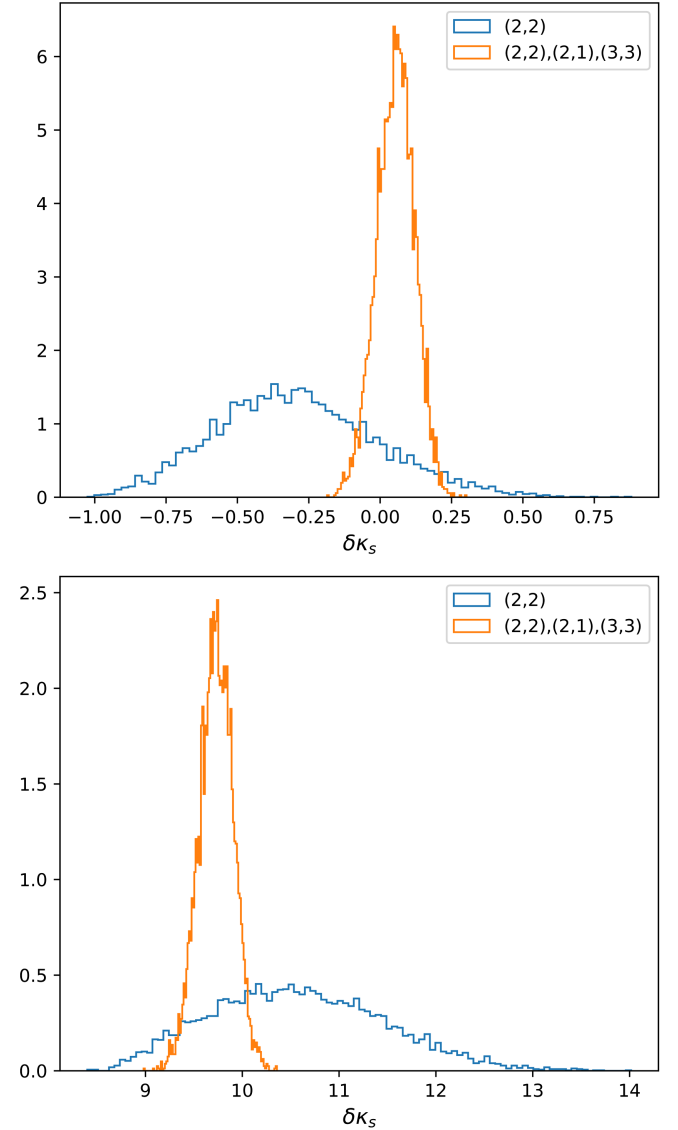


FIG. 2. The PDF of $\delta\kappa_s$ for the waveform with the (2, S2) mode only (blue line) and with higher modes (orange line). The top panel shows the result for the injected signal with higher modes and $\delta\kappa_s = 0$. The bottom panel shows the result for the injected signal with higher modes and $\delta\kappa_s = 10$.

used in the pipeline of data analysis. Moreover, we also assumed that the signal of MBHB has already been detected with the search pipeline such as [92], and all the analysis we did in this work is just parameter estimation [93] and model selection. Both injections have three primary modes: (2, 2), (2, 1), and (3, 3), with all the parameters selected according to Table I. For the waveform used in the matched filtering, we did not assume the model of BBH, which means that $\delta\kappa$ is also a parameter that needs to be estimated and cannot be set as a constant. The marginalized

probability distribution functions (PDFs) are shown in Fig. 2. The results show that, by incorporating the higher modes in the waveform, the capability will be improved for about 3 times. The PE result for all parameters with BBH injection is illustrated in Fig. 3 as an example. We can see that all the parameters are estimated properly, which indicated that all true values are contained in the $1\text{-}\sigma$ region.

We also analyzed the case of a non-BBH injection with the estimation of BBH waveform. The injected value is $\delta\kappa = 10$, and it is fixed to be 0 in the Bayesian analysis.

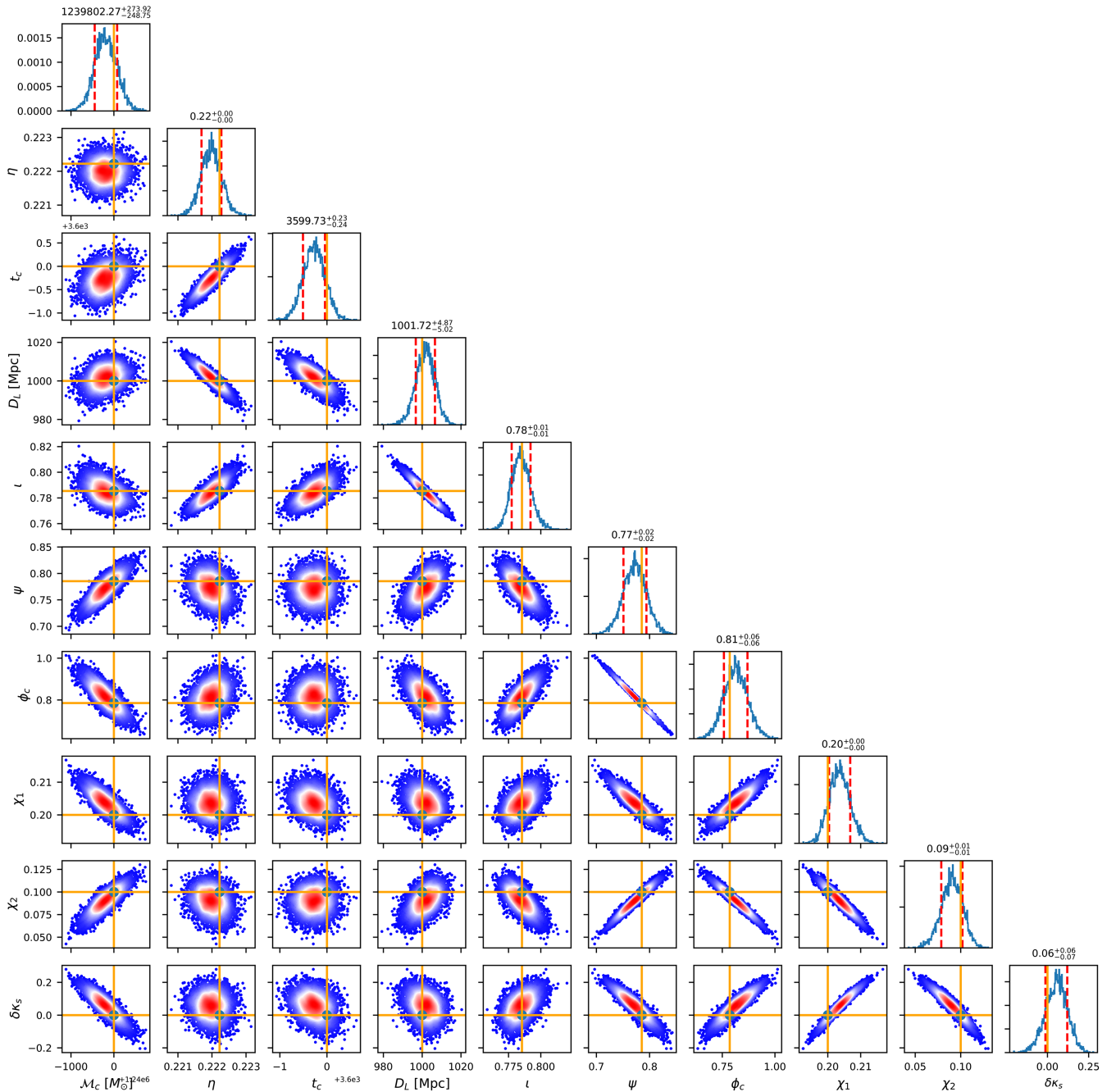


FIG. 3. The PE result with higher modes included waveform, for the injected signal with higher modes and $\delta\kappa_s = 0$. The SIQM is included in the estimated parameters.

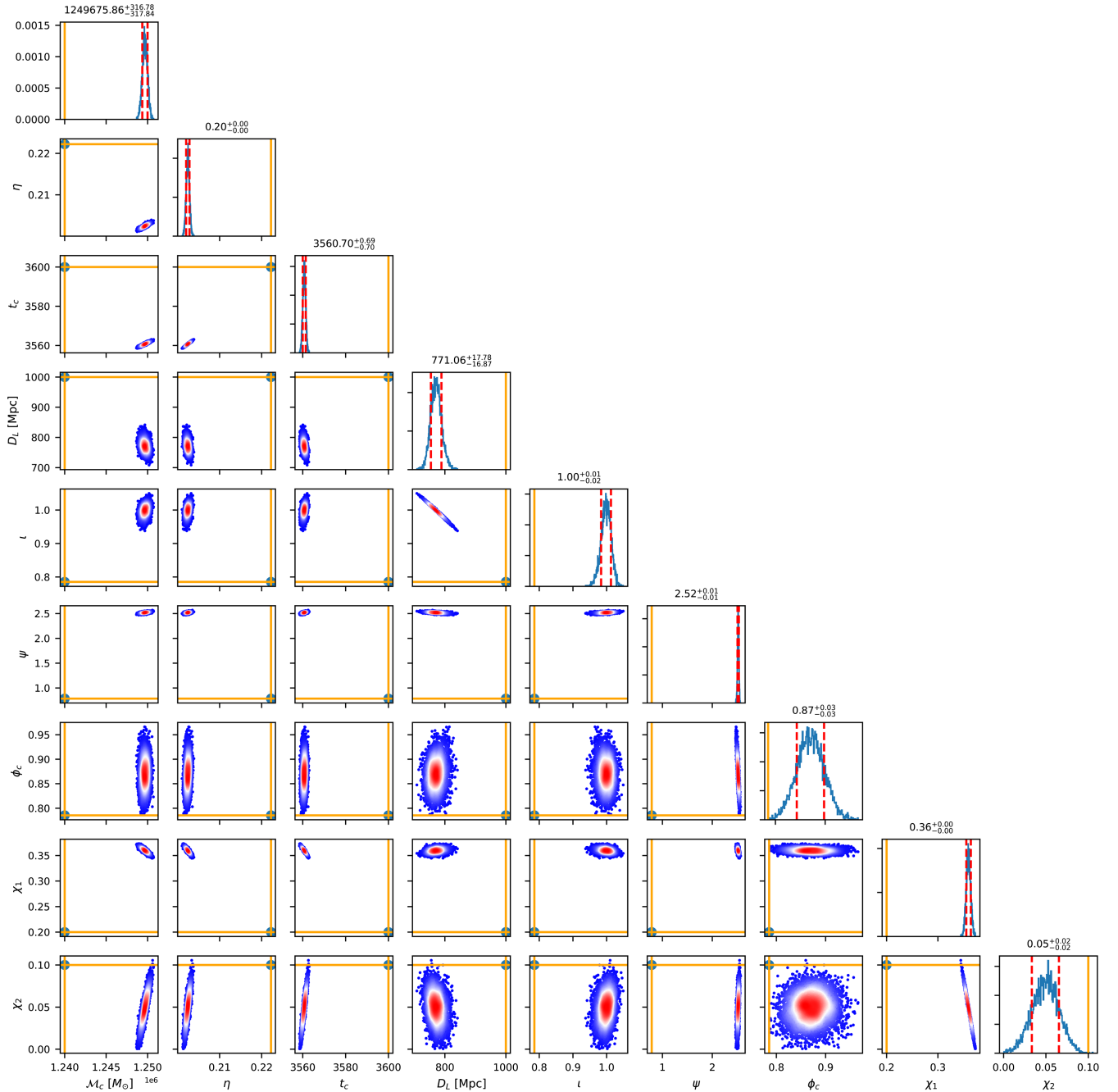


FIG. 4. This figure demonstrates that the corner plots of the waveform template are consistent with $\delta\kappa_s = 0$, but the injected signal has $\delta\kappa_s = 10$ with three modes considered. We can easily notice that the estimated central values deviate from the injected values. This implies that our hypothesis in this figure is incorrect.

This corresponds to a scenario where the data are generated by a binary BS system, but we incorrectly use a BBH waveform to analyze it. The PE result is shown in Fig. 4. We can see that all the parameters are estimated with a significant bias. For example, the injected value of the chirp mass is $1.24 \times 10^6 M_\odot$, but the estimated result is $1.25 \times 10^6 {}^{+160}_{-163} M_\odot$; the true value is approximately $60 - \sigma$ away from the point with the highest likelihood. This

means that, if we use the BBH waveform to fit a binary ECO signal, the parameters we estimate will deviate significantly from the real values.

We also calculate the Bayes factors for the BH hypothesis compared to the ECO hypothesis. Here, we analyzed two types of injections: one with $\delta\kappa_s = 0$ representing the BH, the other with $\delta\kappa_s = 10$ representing the BS. The Bayes factor is calculated according to (19) for model 1 corresponding to BH and model 2 corresponding to ECO.

TABLE III. This table displays the $\lg \text{BF}_{\text{ECO}}^{\text{BH}}$ with an injected signal where $\delta\kappa_s = 0$ or 10, with or without consideration of higher modes.

Injected $\delta\kappa_s$	(2, 2) mode only	Include higher modes
0	0.19	1.49
10	-188.05	-4740.35

Both injections include the higher modes. We consider the case of estimation with only the (2, 2) mode and the case where higher modes are included.

For the injection of BH, the results will support the BH hypothesis, but the Bayes factor is not very large. $\log \text{BF}_{\text{ECO}}^{\text{BH}}$ will be 0.19 if we consider only the (2, 2) mode, and the support for the true model is weak. But the result will increase to 1.49 if we consider the higher modes, and the support for the true model is strong. For the injection of ECO, the results will strongly support the ECO hypothesis, and the Bayes factor will become very large. $\log \text{BF}_{\text{ECO}}^{\text{BH}}$ will be -188.05 if we consider only the (2, 2) mode, and it will become -4740.35 if we consider the higher modes. Both results will support the true model with very strong evidence, as the results shown in Table III. This means that we can distinguish between the BH and ECO models by calculating the Bayes factor, which can help us avoid potential systematic errors.

IV. CONCLUSION

The no-hair theorem states that the multiple moments of a BH are entirely determined by its mass and spin, and it will be violated for ECOs. This work focuses on testing the no-hair theorem by probing the SIQM of the BHs using the inspiral signal of a BBH system. We consider the space-based GW detector TianQin as an example, and then the source chosen is the MBHBs.

With the analysis using the Fisher matrix, we find that TianQin has the best capability for sources with a total mass around $10^{5.5} M_{\odot}$, corresponding to the sensitive band of TianQin. For LISA [49], the best capability total mass is around $2 \times 10^6 M_{\odot}$, and both can constrain their appropriate MBHBs sources' SIQMs to $\mathcal{O}(10^{-1})$ order. Our results also show that BBHBs with a larger mass ratio will have better constraints, indicating the need to consider higher modes.

Then we conducted the analysis using Bayesian inference. The result agrees with the estimation using the Fisher matrix for both the BH and ECO models. The accuracy will improve by about 3 times if we include the higher modes. When using the BH model to infer the parameters of a binary ECO system, we also observe that the estimation of the parameters will have significant systematic errors. However, this can be avoided by calculating the Bayes factor, which will provide strong evidence to distinguish between different models.

As a preliminary exploration, our work still has some limitations. For example, in the model with a nonzero $\delta\kappa$, we have assumed that both ECOs in the binary system have the same value of $\delta\kappa$, and, thus, $\delta\kappa_a$ is fixed at zero. Obviously, this could not be the case in the real world, but the degeneracy between the parameters restricts us from estimating $\delta\kappa_s$ and $\delta\kappa_a$ simultaneously. Moreover, we use the data for only 1 day to perform the PE to reduce the computation, although we have proven that this does not compromise the generality, and the results will not vary significantly for longer datasets. But this is not the case for real data analysis, and the position of the source cannot be estimated in this scenario. We leave the inclusion and treatment of these more realistic issues for future exploration.

ACKNOWLEDGMENTS

The authors thank Yi-Ming Hu, Jiangjin Zheng, Xiangyu Lv, and MengKe Ning for their helpful discussion. We acknowledge the usage of the calculation utilities of BILBY [85], NUMPY [94], and SCIPY [95] and plotting utilities of MATPLOTLIB [96] and CORNER [97]. This work is supported by the Guangdong Basic and Applied Basic Research Foundation (Grant No. 2023A1515030116), the Guangdong Major Project of Basic and Applied Basic Research (Grant No. 2019B030302001), and the National Science Foundation of China (Grant No. 12261131504). This work uses BILBY.

APPENDIX: THE FREQUENCY FOR ISCO

In this appendix, we present the formula corresponding the ISCO frequency for BBH with spin [98]. The ISCO frequency can be written as

$$f_{\text{ISCO}} = \frac{\hat{\Omega}(\chi_f)}{\pi M_f}, \quad (\text{A1})$$

where χ_f represents the final spin and M_f represents the final mass of the remnant BH after the merger of BBHBs. The detailed calculation can be found in Refs. [99,100]. $\hat{\Omega}(\chi_f)$ represents the dimensionless ISCO Kerr angular frequency:

$$\hat{\Omega}(\chi_f) = \frac{1}{\hat{r}_{\text{ISCO}}^{3/2}(\chi_f) + \chi_f}. \quad (\text{A2})$$

The dimensionless radius of the ISCO for a Kerr BH with a dimensionless spin parameter χ is

$$\begin{aligned} \hat{r}_{\text{ISCO}}(\chi) &= 3 + Z_2 - \frac{\chi}{|\chi|} \sqrt{(3 - Z_1)(3 + Z_1 + 2Z_2)}, \\ Z_2 &= \sqrt{3\chi^2 + Z_1^2}, \\ Z_1 &= 1 + (1 - \chi^2)^{1/3}((1 + \chi)^{1/3} + (1 - \chi)^{1/3}). \end{aligned} \quad (\text{A3})$$

- [1] B. P. Abbott, R. Abbott, T. Abbott, M. Abernathy, F. Acernese, K. Ackley, C. Adams, T. Adams, P. Addesso, R. Adhikari *et al.*, *Phys. Rev. Lett.* **116**, 131103 (2016).
- [2] R. Abbott, T. Abbott, S. Abraham, F. Acernese, K. Ackley, A. Adams, C. Adams, R. Adhikari, V. Adya, C. Affeldt *et al.*, *Phys. Rev. X* **11**, 021053 (2021).
- [3] R. Abbott *et al.*, *Astrophys. J.* **949**, 76 (2023).
- [4] L. Scientific, *Phys. Rev. D* **109**, 022001 (2024).
- [5] B. Abbott, R. Abbott, T. Abbott, S. Abraham, F. Acernese, K. Ackley, C. Adams, R. X. Adhikari, V. Adya, C. Affeldt *et al.*, *Phys. Rev. D* **100**, 104036 (2019).
- [6] F. S. Broekgaarden and E. Berger, *Astrophys. J. Lett.* **920**, L13 (2021).
- [7] N. K. Johnson-McDaniel, A. Mukherjee, R. Kashyap, P. Ajith, W. Del Pozzo, and S. Vitale, *Phys. Rev. D* **102**, 123010 (2020).
- [8] P. Haensel, J. Zdukun, and R. Schaefer, *Astron. Astrophys.* **160**, 121 (1986).
- [9] E. W. Kolb and I. I. Tkachev, *Phys. Rev. Lett.* **71**, 3051 (1993).
- [10] P. O. Mazur and E. Mottola, *Universe* **9**, 88 (2023).
- [11] V. Cardoso and P. Pani, *Living Rev. Relativity* **22**, 1 (2019).
- [12] S. W. Hawking, *Phys. Rev. D* **72**, 084013 (2005).
- [13] R. D. Blandford and R. L. Znajek, *Mon. Not. R. Astron. Soc.* **179**, 433 (1977).
- [14] T. Hinderer, B. D. Lackey, R. N. Lang, and J. S. Read, *Phys. Rev. D* **81**, 123016 (2010).
- [15] K. Chatziioannou, *Gen. Relativ. Gravit.* **52**, 109 (2020).
- [16] C. A. Raithel, F. Özel, and D. Psaltis, *Astrophys. J. Lett.* **857**, L23 (2018).
- [17] T. Malik, N. Alam, M. Fortin, C. Providência, B. Agrawal, T. Jha, B. Kumar, and S. Patra, *Phys. Rev. C* **98**, 035804 (2018).
- [18] S. Bernuzzi, A. Nagar, and A. Zenginoğlu, *Phys. Rev. D* **86**, 104038 (2012).
- [19] K. D. Kokkotas and B. G. Schmidt, *Living Rev. Relativity* **2**, 1 (1999).
- [20] B. J. Kelly and J. G. Baker, *Phys. Rev. D* **87**, 084004 (2013).
- [21] I. Ota and C. Chirenti, *Phys. Rev. D* **101**, 104005 (2020).
- [22] V. Baibhav, E. Berti, V. Cardoso, and G. Khanna, *Phys. Rev. D* **97**, 044048 (2018).
- [23] C. Shi, J. Bao, H.-T. Wang, J.-d. Zhang, Y.-M. Hu, A. Sesana, E. Barausse, J. Mei, and J. Luo, *Phys. Rev. D* **100**, 044036 (2019).
- [24] E. Berti, V. Cardoso, and C. M. Will, *Phys. Rev. D* **73**, 064030 (2006).
- [25] E. Berti, J. Cardoso, V. Cardoso, and M. Cavaglia, *Phys. Rev. D* **76**, 104044 (2007).
- [26] O. Dreyer, B. Kelly, B. Krishnan, L. S. Finn, D. Garrison, and R. Lopez-Aleman, *Classical Quantum Gravity* **21**, 787 (2004).
- [27] S. Detweiler, *Astrophys. J.* **239**, 292 (1980).
- [28] E. Poisson, *Phys. Rev. D* **57**, 5287 (1998).
- [29] S. Kastha, A. Gupta, K. Arun, B. Sathyaprakash, and C. Van Den Broeck, *Phys. Rev. D* **98**, 124033 (2018).
- [30] R. O. Hansen, *J. Math. Phys. (N.Y.)* **15**, 46 (1974).
- [31] R. Geroch, *J. Math. Phys. (N.Y.)* **11**, 2580 (1970).
- [32] K. S. Thorne, *Rev. Mod. Phys.* **52**, 299 (1980).
- [33] G. Compere, R. Oliveri, and A. Seraj, *J. High Energy Phys.* **05** (2018) 054.
- [34] N. Krishnendu, K. Arun, and C. K. Mishra, *Phys. Rev. Lett.* **119**, 091101 (2017).
- [35] W. G. Laarakkers and E. Poisson, *Astrophys. J.* **512**, 282 (1999).
- [36] G. Pappas and T. A. Apostolatos, *Phys. Rev. Lett.* **108**, 231104 (2012).
- [37] L. C. Stein, K. Yagi, and N. Yunes, *Astrophys. J.* **788**, 15 (2014).
- [38] C. A. Herdeiro and E. Radu, *Phys. Rev. Lett.* **112**, 221101 (2014).
- [39] D. Baumann, H. S. Chia, and R. A. Porto, *Phys. Rev. D* **99**, 044001 (2019).
- [40] N. Uchikata, S. Yoshida, and P. Pani, *Phys. Rev. D* **94**, 064015 (2016).
- [41] F. Dubeibe, L. A. Pachón, and J. D. Sanabria-Gómez, *Phys. Rev. D* **75**, 023008 (2007).
- [42] F. D. Ryan, *Phys. Rev. D* **56**, 1845 (1997).
- [43] F. D. Ryan, *Phys. Rev. D* **55**, 6081 (1997).
- [44] T. Narikawa, N. Uchikata, and T. Tanaka, *Phys. Rev. D* **104**, 084056 (2021).
- [45] N. V. K. Divyajyoti, *Phys. Rev. D* **109**, 023016 (2024).
- [46] P. Saini and N. V. Krishnendu, *Phys. Rev. D* **109**, 024009 (2024).
- [47] R. Abbott, H. Abe, F. Acernese, K. Ackley, N. Adhikari, R. Adhikari, V. Adkins, V. Adya, C. Affeldt, D. Agarwal *et al.*, [arXiv:2112.06861](https://arxiv.org/abs/2112.06861).
- [48] R. Abbott, T. Abbott, S. Abraham, F. Acernese, K. Ackley, A. Adams, C. Adams, R. X. Adhikari, V. Adya, C. Affeldt *et al.*, *Phys. Rev. D* **103**, 122002 (2021).
- [49] N. Krishnendu and A. B. Yelikar, *Classical Quantum Gravity* **37**, 205019 (2020).
- [50] H.-M. Fan, Y.-M. Hu, E. Barausse, A. Sesana, J.-d. Zhang, X. Zhang, T.-G. Zi, and J. Mei, *Phys. Rev. D* **102**, 063016 (2020).
- [51] T. Zi, J.-d. Zhang, H.-M. Fan, X.-T. Zhang, Y.-M. Hu, C. Shi, and J. Mei, *Phys. Rev. D* **104**, 064008 (2021).
- [52] M. Liu and J.-d. Zhang, [arXiv:2008.11396](https://arxiv.org/abs/2008.11396).
- [53] L. Barack and C. Cutler, *Phys. Rev. D* **69**, 082005 (2004).
- [54] L. Barack and C. Cutler, *Phys. Rev. D* **75**, 042003 (2007).
- [55] S. Babak, J. Gair, A. Sesana, E. Barausse, C. F. Sopuerta, C. P. Berry, E. Berti, P. Amaro-Seoane, A. Petiteau, and A. Klein, *Phys. Rev. D* **95**, 103012 (2017).
- [56] M. Rahman and A. Bhattacharyya, *Phys. Rev. D* **107**, 024006 (2023).
- [57] J. Luo, L.-S. Chen, H.-Z. Duan, Y.-G. Gong, S. Hu, J. Ji, Q. Liu, J. Mei, V. Milyukov, M. Sazhin *et al.*, *Classical Quantum Gravity* **33**, 035010 (2016).
- [58] Y.-M. Hu, J. Mei, and J. Luo, *Natl. Sci. Rev.* **4**, 683 (2017).
- [59] J. Mei, Y.-Z. Bai, J. Bao, E. Barausse, L. Cai, E. Canuto, B. Cao, W.-M. Chen, Y. Chen, Y.-W. Ding *et al.*, *Prog. Theor. Exp. Phys.* **2021**, 05A107 (2021).
- [60] H.-T. Wang, Z. Jiang, A. Sesana, E. Barausse, S.-J. Huang, Y.-F. Wang, W.-F. Feng, Y. Wang, Y.-M. Hu, J. Mei *et al.*, *Phys. Rev. D* **100**, 043003 (2019).
- [61] W.-F. Feng, H.-T. Wang, X.-C. Hu, Y.-M. Hu, and Y. Wang, *Phys. Rev. D* **99**, 123002 (2019).
- [62] S. Liu, Y.-M. Hu, J.-d. Zhang, and J. Mei *et al.*, *Phys. Rev. D* **101**, 103027 (2020).

- [63] S. Liu, L.-G. Zhu, Y.-M. Hu, J.-D. Zhang, and M.-J. Ji, *Phys. Rev. D* **105**, 023019 (2022).
- [64] S.-J. Huang, Y.-M. Hu, V. Korol, P.-C. Li, Z.-C. Liang, Y. Lu, H.-T. Wang, S. Yu, and J. Mei, *Phys. Rev. D* **102**, 063021 (2020).
- [65] H.-M. Fan, S. Zhong, Z.-C. Liang, Z. Wu, J.-d. Zhang, and Y.-M. Hu, *Phys. Rev. D* **106**, 124028 (2022).
- [66] Z.-C. Liang, Z.-Y. Li, E.-K. Li, J.-d. Zhang, and Y.-M. Hu, [arXiv:2307.01541](https://arxiv.org/abs/2307.01541).
- [67] Z.-C. Liang, Y.-M. Hu, Y. Jiang, J. Cheng, J.-d. Zhang, and J. Mei, *Phys. Rev. D* **105**, 022001 (2022).
- [68] L.-G. Zhu, Y.-M. Hu, H.-T. Wang, J.-d. Zhang, X.-D. Li, M. Hendry, and J. Mei, *Phys. Rev. Res.* **4**, 013247 (2022).
- [69] L.-G. Zhu, L.-H. Xie, Y.-M. Hu, S. Liu, E.-K. Li, N. R. Napolitano, B.-T. Tang, J.-d. Zhang, and J. Mei, *Sci. China Phys. Mech. Astron.* **65**, 259811 (2022).
- [70] S.-J. Huang, Y.-M. Hu, X. Chen, J.-d. Zhang, E.-K. Li, Z. Gao, and X.-Y. Lin, *J. Cosmol. Astropart. Phys.* **08** (2023) 003.
- [71] J. Bao, C. Shi, H. Wang, J.-d. Zhang, Y. Hu, J. Mei, and J. Luo, *Phys. Rev. D* **100**, 084024 (2019).
- [72] S. Sun, C. Shi, J.-d. Zhang, and J. Mei, *Phys. Rev. D* **107**, 044023 (2023).
- [73] N. Xie, J.-d. Zhang, S.-J. Huang, Y.-M. Hu, and J. Mei, *Phys. Rev. D* **106**, 124017 (2022).
- [74] C. Shi, M. Ji, J.-d. Zhang, and J. Mei, *Phys. Rev. D* **108**, 024030 (2023).
- [75] X.-y. Lin, J.-d. Zhang, L. Dai, S.-J. Huang, and J. Mei, *Phys. Rev. D* **108**, 064020 (2023).
- [76] C. García-Quirós, M. Colleoni, S. Husa, H. Estellés, G. Pratten, A. Ramos-Buades, M. Mateu-Lucena, and R. Jaume, *Phys. Rev. D* **102**, 064002 (2020).
- [77] K. Arun, A. Buonanno, G. Faye, and E. Ochsner, *Phys. Rev. D* **79**, 104023 (2009).
- [78] C. K. Mishra, A. Kela, K. Arun, and G. Faye, *Phys. Rev. D* **93**, 084054 (2016).
- [79] S. Mezzasoma and N. Yunes, *Phys. Rev. D* **106**, 024026 (2022).
- [80] M. Tinto, F. B. Estabrook, and J. W. Armstrong, *Phys. Rev. D* **69**, 082001 (2004).
- [81] S. Marsat, J. G. Baker, and T. Dal Canton, *Phys. Rev. D* **103**, 083011 (2021).
- [82] X. Lyu, E.-K. Li, and Y.-M. Hu, *Phys. Rev. D* **108**, 083023 (2023).
- [83] C. Cutler and E. E. Flanagan, *Phys. Rev. D* **49**, 2658 (1994).
- [84] E. Thrane and C. Talbot, *Pub. Astron. Soc. Aust.* **36**, e010 (2019).
- [85] G. Ashton, M. Hübner, P. D. Lasky, C. Talbot, K. Ackley, S. Biscoveanu, Q. Chu, A. Divakarla, P. J. Easter, B. Goncharov *et al.*, *Astrophys. J. Suppl. Ser.* **241**, 27 (2019).
- [86] J. S. Speagle, *Mon. Not. R. Astron. Soc.* **493**, 3132 (2020).
- [87] J. Skilling, *Bayesian Anal.* **1**, 833 (2006).
- [88] A. Torres-Orjuela, S.-J. Huang, Z.-C. Liang, S. Liu, H.-T. Wang, C.-Q. Ye, Y.-M. Hu, and J. Mei, [arXiv:2307.16628](https://arxiv.org/abs/2307.16628).
- [89] B. Wang, C. Shi, J.-d. Zhang, Y.-M. hu, and J. Mei, *Phys. Rev. D* **108**, 044061 (2023).
- [90] T. B. Littenberg and N. J. Cornish, *Phys. Rev. D* **107**, 063004 (2023).
- [91] M. L. Katz, N. Karnesis, N. Korsakova, J. R. Gair, and N. Stergioulas, [arXiv:2405.04690](https://arxiv.org/abs/2405.04690).
- [92] H.-Y. Chen, X.-Y. Lyu, E.-K. Li, and Y.-M. Hu, *Sci. China Phys. Mech. Astron.* **67**, 279512 (2024).
- [93] J. Gao, Y.-M. Hu, E.-K. Li, J.-d. Zhang, and J. Mei, [arXiv:2401.12813](https://arxiv.org/abs/2401.12813).
- [94] S. van der Walt, S. C. Colbert, and G. Varoquaux, *Comput. Sci. Eng.* **13**, 22 (2011).
- [95] P. Virtanen *et al.*, *Nat. Methods* **17**, 261 (2020).
- [96] J. D. Hunter, *Comput. Sci. Eng.* **9**, 90 (2007).
- [97] D. Foreman-Mackey, *J. Open Source Software* **1**, 24 (2016).
- [98] M. Favata, C. Kim, K. Arun, J. Kim, and H. W. Lee, *Phys. Rev. D* **105**, 023003 (2022).
- [99] S. Husa, S. Khan, M. Hannam, M. Pürrer, F. Ohme, X. J. Forteza, and A. Bohé, *Phys. Rev. D* **93**, 044006 (2016).
- [100] F. Hofmann, E. Barausse, and L. Rezzolla, *Astrophys. J. Lett.* **825**, L19 (2016).